

Using high multipolar orders to reconstruct the sound velocity in piezoelectrics from lattice dynamics

Miquel Royo,^{1,*} Konstanze R. Hahn,¹ and Massimiliano Stengel^{1,2,†}

¹*Institut de Ciència de Materials de Barcelona (ICMAB-CSIC), Campus UAB, 08193 Bellaterra, Spain*

²*ICREA - Institució Catalana de Recerca i Estudis Avançats, 08010 Barcelona, Spain*

(Dated: March 1, 2022)

Information over the phonon band structure is crucial to predicting many thermodynamic properties of materials, such as thermal transport coefficients. Highly accurate phonon dispersion curves can be, in principle, calculated in the framework of density-functional perturbation theory (DFPT). However, well-established techniques can run into trouble (or even catastrophically fail) in the case of piezoelectric materials, where the acoustic branches hardly reproduce the physically correct sound velocity. Here we identify the culprit in the higher-order multipolar interactions between atoms, and demonstrate an effective procedure that fixes the aforementioned issue. Our strategy drastically improves the predictive power of perturbative lattice-dynamical calculations in piezoelectric crystals, and is directly implementable for high-throughput generation of materials databases.

The distribution of vibrational frequencies as a function of crystal momentum, known as the phonon band structure, is a key physical property of crystals. Its accurate knowledge is central to predicting several technologically important functionalities, such as thermal expansion [1] and thermoelectric [2–6] coefficients, specific heat, [7, 8] electron-phonon scattering [9], etc. In many cases, the low-energy part of the phonon spectrum, consisting of acoustic waves, dominates the aforementioned properties at low to intermediate temperatures. Therefore, for making quantitatively accurate predictions, it is important that the dispersion of the corresponding phonon branches matches the correct sound velocity in a given material.

Density functional perturbation theory (DFPT) [10–13] has become the state-of-the-art method to calculate the phonon spectrum of crystalline solids from first principles. It allows one to calculate the dynamical matrix, at a computational cost that does not depend on the wavevector \mathbf{q} , via the second derivatives of the energy with respect to atomic displacements; subsequent diagonalization yields then the relevant phonon frequencies. Such a procedure could, in principle, be repeated on an arbitrarily dense mesh of \mathbf{q} -vectors to integrate the desired thermodynamic function over the full Brillouin zone. This, however, is often impractical; typically, the explicit calculation of the dynamical matrix is carried out on a relatively coarse \mathbf{q} -mesh only, and later Fourier-interpolated to a finer grid for thermodynamic integration.

To ensure an accurate interpolation in polar materials, it is crucial to separate the interatomic force constants (IFCs) into a long-ranged dipole-dipole (DD) interaction, which decays as the inverse third power of the interatomic distance d , and a “short-ranged” (SR) part, which is simply defined as the remainder. The DD part can be exactly written in terms of two basic ingredients, the Born effective charge tensor (\mathbf{Z}^*) and the macroscopic dielectric tensor ϵ_∞ [13–16]; both can be routinely calculated

nowadays for an arbitrary insulator by means of publicly available simulation packages. The SR part, in turn, is assumed to decay sufficiently fast (DD terms indeed constitute the leading contribution at large distances) as a function of d that its Fourier interpolation is efficient and accurate for most purposes.

This procedure yields excellent results in the vast majority of practical cases. The main physical consequence of the DD interactions, namely the frequency splitting between transverse (TO) and longitudinal (LO) optical phonons at Γ , [17] is exactly reproduced by construction. Other features of the phonon spectrum typically show optimal convergence even by using relatively coarse \mathbf{q} -point meshes. [13] Nevertheless, a number of cases have been reported over the years where unphysical features appear in the interpolated band structures, notably regarding the low-energy bands near the zone center. For example, Refs. [18, 19] studied the lattice-dynamical properties of SiO_2 across the phase transition from shistovite to CaCl_2 structure, finding spurious imaginary acoustic modes in a broad range of pressures around the critical value. Similar imaginary modes can be appreciated in Ref. 20 for α -quartz GeO_2 and in numerous phonon band structures of piezoelectrics accessible through material databases (see, e.g., KNbO_3 , PNO, BeSO_4 , PdF_4 , BPO_4 or GaPO_4 in Ref. 21). While the aforementioned artifacts were initially ascribed to numerical issues [18] (i.e. to a lack of convergence with respect to the relevant computational parameters), later studies leaned towards a systematic error of the Fourier interpolation scheme. [19] The nature of this error, however, hasn’t been clarified yet.

Here we propose an improved scheme for the Fourier interpolation of phonon bands in insulators, where long-range forces associated to higher-order multipolar terms (dipole-quadrupole, quadrupole-quadrupole, dipole-octupole and dielectric dispersion effects) are explicitly treated next to the usual dipole-dipole interactions. Based on analytical derivations and numerical tests we show that this generalization is essential for a

reliable description of the phonon dispersion around the Brillouin zone center. In particular, by using ferroelectric BaTiO₃ as a testcase, we demonstrate an extremely rapid convergence of the acoustic branches to the physically correct sound velocity, while spurious imaginary modes are present in the band structure calculated by ordinary means. These unstable modes, which are an artefact of the established Fourier interpolation scheme, persist even in the limit of dense meshes, and would thwart any attempt at computing thermodynamic integrals based on such data. Remarkably, our new scheme yields well-behaved (i.e. real) frequencies even in the coarsest $2 \times 2 \times 2$ meshes that we have tested.

The treatment of the acoustic phonons starting from microscopic lattice dynamics occupies an extensive portion of Born and Huang's book, [22] and has been revised and extended very recently in the context of flexoelectricity. [23, 24] We shall start with reviewing the results that are most relevant for the present context. The basic ingredient is the dynamical matrix (Φ) at some wavevector \mathbf{q} , defined as the second derivative of the total energy (E) with respect to two monochromatic perturbations,

$$\Phi_{\kappa\alpha, \kappa'\beta}^{\mathbf{q}} = \frac{\partial^2 E}{\partial u_{\kappa\alpha}^{\mathbf{q}*} \partial u_{\kappa'\beta}^{\mathbf{q}}}, \quad u_{\kappa\alpha}^l = u_{\kappa\alpha}^{\mathbf{q}} e^{i\mathbf{q} \cdot \mathbf{R}_{l\kappa}}. \quad (1)$$

Here κ and κ' are sublattice indices, l is a cell index, the real-space vectors $\mathbf{R}_{l\kappa} = \mathbf{R}_l + \boldsymbol{\tau}_\kappa$ span the crystal lattice, and $\alpha\beta$ are Cartesian directions. Then, the acoustic eigenmodes and velocities can be derived [22–24] by performing a perturbative expansion in \mathbf{q} of the lattice-dynamical problem

$$\sum_{\kappa'\beta} \Phi_{\kappa\alpha\kappa'\beta}^{\mathbf{q}} u_{\kappa'\beta}^{\mathbf{q}} = \omega^2 m_\kappa u_{\kappa\alpha}^{\mathbf{q}}, \quad (2)$$

where m_κ are atomic masses, ω is the frequency, and $u_{\kappa\alpha}^{\mathbf{q}}$ are the mode eigenvectors. Following Ref. 24, we shall write $\mathbf{q} = q\hat{\mathbf{q}}$ and take the perturbation expansion in the modulus of the wave vector, q , while keeping the direction $\hat{\mathbf{q}}$ fixed. The dynamical matrix at small q then reads as

$$\Phi^{\mathbf{q}} = \Phi^{(0,\hat{\mathbf{q}})} - iq\Phi^{(1,\hat{\mathbf{q}})} - \frac{q^2}{2}\Phi^{(2,\hat{\mathbf{q}})} + \dots \quad (3)$$

Eq. (2) in turn becomes, at second order in q ,

$$\left(K_{jl}^{\hat{\mathbf{q}}} - Mv^2\delta_{jl} \right) u_l = 0, \quad (4)$$

where v is the sound velocity, M is the total mass of the cell, \mathbf{u} is the polarization of the phonon branch, and \mathbf{K} is defined as

$$K_{jl}^{\hat{\mathbf{q}}} = -\frac{1}{2}\Phi^{(2,\hat{\mathbf{q}})} + \Phi^{(1,\hat{\mathbf{q}})} \cdot \tilde{\Phi}^{(0,\hat{\mathbf{q}})} \cdot \Phi^{(1,\hat{\mathbf{q}})}, \quad (5)$$

$$K_{jl}^{\hat{\mathbf{q}}} = \sum_{\kappa\kappa'} \langle \kappa j | K^{\hat{\mathbf{q}}} | \kappa' l \rangle. \quad (6)$$

$\tilde{\Phi}^{(0,\hat{\mathbf{q}})}$ denotes the pseudoinverse of the zone-center dynamical matrix; open-circuit electrical boundary conditions are assumed along $\hat{\mathbf{q}}$ for all quantities in Eq. (5).

After careful considerations of the nonanalytic behavior of $\Phi^{\mathbf{q}}$ near the zone center, we find [25]

$$K_{jl}^{\hat{\mathbf{q}}} = \Omega \sum_{ik} \hat{q}_i \cdot C_{ijkl}^{\hat{\mathbf{q}}} \cdot \hat{q}_k. \quad (7)$$

where $\mathbf{C}^{\hat{\mathbf{q}}}$ is the elastic tensor in “mixed electrical boundary conditions” [26, 27] (open circuit is imposed along $\hat{\mathbf{q}}$),

$$C_{ijkl}^{\hat{\mathbf{q}}} = C_{ijkl} + 4\pi \frac{(\hat{\mathbf{q}} \cdot \mathbf{e})_{ij} (\hat{\mathbf{q}} \cdot \mathbf{e})_{kl}}{\hat{\mathbf{q}} \cdot \boldsymbol{\epsilon} \cdot \hat{\mathbf{q}}}, \quad (8)$$

Here \mathbf{C} is the elastic tensor calculated in short-circuit, and the second term on the rhs embodies the direction-dependent macroscopic electric field contribution via the piezoelectric (\mathbf{e}) and dielectric ($\boldsymbol{\epsilon}$) tensors. (All three tensors are defined in the static limit, i.e. inclusive of lattice-mediated contributions.) Thus, Eq.(4) exactly reduces to the macroscopic Christoffel equation [28, 29] for sound waves in a crystalline insulator of arbitrary symmetry.

The above derivations establish the formal connection between macroscopic elasticity and microscopic lattice dynamics by generalizing the classic arguments of Born and Huang [22] to an arbitrary crystal, including polar and piezoelectric insulators. The link between long-wavelength phonons and Eq. (8) is provided by Martin's formula [30] for the macroscopic piezoelectric tensor, where the latter is written in terms of dynamical dipoles and quadrupoles associated to atomic displacements. Thus, from these derivations we have learned a crucially important fact: to reproduce the correct sound velocity in a phonon band structure calculation of a piezoelectric material, higher-order multipolar contributions (e.g., involving dynamical quadrupoles [31]) to the IFCs play a key role.

To see the implications of this statement in the context of first-principles lattice dynamics, we shall recap the state-of-the-art method for the Fourier interpolation of the phonon bands in insulating crystals. $\Phi^{\mathbf{q}}$ is typically calculated within density-functional perturbation theory on a “coarse” mesh of \mathbf{q}_i points spanning the Brillouin zone, and later interpolated on a much finer mesh for computing various thermodynamic quantities. To this end, one first defines a “long-range” (LR) dipole-dipole contribution in terms of the Born effective charge and dielectric tensors, and subtracts it from the calculated $\Phi(\mathbf{q}_i)$,

$$\Phi^{\text{SR}}(\mathbf{q}_i) = \Phi(\mathbf{q}_i) - \Phi^{\text{LR}}(\mathbf{q}_i). \quad (9)$$

Next, the remainder “short-range” (SR) part is backward Fourier-transformed to obtain the real-space interatomic force constants (IFC) on a supercell, \mathcal{S} , that is dual to

the coarse \mathbf{q} -mesh. (\mathcal{S} is assumed to be a polyhedron centered at the origin; the IFC are conveniently truncated at the boundaries according to the interatomic distance.) Finally, the dynamical matrix at an arbitrary point \mathbf{q} is reconstructed by adding back the dipole-dipole term to the Fourier-interpolated (IN) short-range part,

$$\Phi^{\text{tot}}(\mathbf{q}) = \Phi^{\text{IN}}(\mathbf{q}) + \Phi^{\text{LR}}(\mathbf{q}), \quad (10)$$

where the latter are defined as

$$\Phi_{\kappa\alpha,\kappa'\beta}^{\text{IN},\mathbf{q}} = \sum_{l: \mathbf{d}_{\kappa\kappa'}^l \in \mathcal{S}} \Phi_{\kappa\alpha,\kappa'\beta}^{\text{SR},l} e^{-i\mathbf{q} \cdot \mathbf{d}_{\kappa\kappa'}^l}. \quad (11)$$

($\mathbf{d}_{\kappa\kappa'}^l = \mathbf{R}_l + \boldsymbol{\tau}_{\kappa'} - \boldsymbol{\tau}_{\kappa}$ is the real-space vector connecting atoms 0κ and $l\kappa'$.)

We can now connect to Eq. (4) by expanding the interpolated dynamical matrix in powers of q , similarly to Eq. (3). We shall specifically focus on $\Phi^{\text{IN},\mathbf{q}}$, since Φ^{LR} is defined by analytical formulas and therefore trivial to deal with in this context. We find that the n -th expansion term is trivially given by the real-space moments of the short-range IFC,

$$\Phi_{\kappa\alpha,\kappa'\beta}^{\text{IN}-(n,\hat{\mathbf{q}})} = \sum_{l: \mathbf{d}_{\kappa\kappa'}^l \in \mathcal{S}} \Phi_{\kappa\alpha,\kappa'\beta}^{\text{SR},l} (\mathbf{d}_{\kappa\kappa'}^l \cdot \hat{\mathbf{q}})^n. \quad (12)$$

The validity of the interpolation procedure for the long-wavelength acoustic waves therefore rests on the accuracy of Eq. (12), and in particular on whether the lattice sums up to $n = 2$ are well-defined. [Eq. (4) contains q -derivatives of the dynamical matrix up to second order.]

A sufficient condition for the n -th moment to converge is that the SR interatomic force constants decay faster than $1/d^{3+n}$, since the sum must be performed over the three-dimensional volume of \mathcal{S} . Thus, in our case we must require that $\Phi_{\kappa\alpha,\kappa'\beta}^{\text{SR},l}$ decay faster than $1/d^5$. Within the standard interpolation method the decay rate, however, is only guaranteed to be faster than $1/d^3$, since the dipole-dipole interactions are subtracted out from the IFC calculated from first principles, but higher-order multipolar interactions (e.g., dipole-quadrupole, decaying as $\sim 1/d^4$) are generally present. As a consequence the lattice sums for $n = 1, 2$ in Eq. (12) are, in principle, only *conditionally convergent*. This means that the sound velocity that one extracts from the interpolated phonon band structure may depend on the details of how the IFCs are truncated at the boundary, i.e. on the *shape* of the supercell \mathcal{S} that one uses in practice. Note that this statement holds *even in the limit of a very large supercell size*, so in severe cases this issue may be difficult or impossible to solve by simply increasing the density of the coarse \mathbf{q} -mesh.

To solve this issue, we shall rewrite the long-range contribution of Eq. (9) and Eq. (10) by incorporating enough terms to reproduce the nonanalyticities of $\Phi(\mathbf{q})$ up to

$O(q^2)$,

$$\begin{aligned} \Phi^{\text{LR}}(\mathbf{q}) = & \Phi^{\text{DD}}(\mathbf{q}) + \Phi^{\text{DQ}}(\mathbf{q}) \\ & + \Phi^{\text{DO}}(\mathbf{q}) + \Phi^{\text{QQ}}(\mathbf{q}) + \Phi^{\text{DeD}}(\mathbf{q}), \end{aligned} \quad (13)$$

Here D, Q and O stand for dipole, quadrupole and octupole respectively. The last term on the rhs (DeD) is a dipole-dipole term mediated by the dielectric dispersion. [25] The modification of the LR part redefines the short-range IFC's as well, which are now guaranteed to decay as $1/d^6$ or faster (all interactions up to $1/d^5$ have been removed), as required by Eq. (5). Interestingly, in addition to the DQ and QQ interactions (whose importance for piezoelectric crystals was formally demonstrated in the earlier paragraphs), we have two additional $O(q^2)$ terms here, DO and DeD, whose significance may be at first sight unclear. If \mathcal{S} were infinitely large, neither interaction should have an impact on the sound velocity – the corresponding electrostatic contributions to the acoustic branches would vanish because of the acoustic sum rule (ASR). [25] Yet, at finite \mathcal{S} size, the abrupt truncation of the IFCs at the boundary might spoil the ASR at the level of the DO and DeD terms, resulting in a slow convergence of the interpolated sound velocity with \mathbf{q} -mesh resolution. We shall see shortly, by using rhombohedral BaTiO₃ as a test case, an excellent practical demonstration of these arguments: while inclusion of dipole-quadrupole terms produces the most dramatic effects, DO and DeD terms further improve the convergence rate of the interpolated sound velocities, and rather substantially so.

We have implemented the above procedure [25] to calculate the higher-order long-range interactions into the ANADDB post-processing program, which is part of the ABINIT suite. (The v9 version of ABINIT with this new functionality has just been released for public use. [32]) The phonon band dispersion evaluated along the path Γ -X-M- Γ -R and calculated with a $4 \times 4 \times 4$ \mathbf{q} -points mesh is represented in Fig.1. Red-dashed lines show the results obtained following the standard procedure, [16, 33] in which $\Phi^{\text{LR}}(\mathbf{q})$ exclusively includes dipole-dipole interactions. The optical bands resulting from this calculation show no visible anomalies. However, a sizeable portion of one of the transverse acoustic (TA) bands dips into imaginary frequencies at the long-wave limit of the Γ -M (corresponding to [110]) segment. Such anomaly does *not* disappear by increasing the density of the coarse \mathbf{q} -mesh – spurious imaginary modes persist along [110] up to the highest-density mesh we could realistically afford ($12 \times 12 \times 12$), as illustrated in Fig. 1(b). To confirm that this artifact is indeed related to the Fourier interpolation scheme, we have performed explicit DFPT calculations of the phonon frequencies at selected (small) \mathbf{q} values along [110], always obtaining real frequencies. Also, this is certainly not the signature of a *physical* ferroelastic instability of the crystal, since the BaTiO₃ cell has been carefully

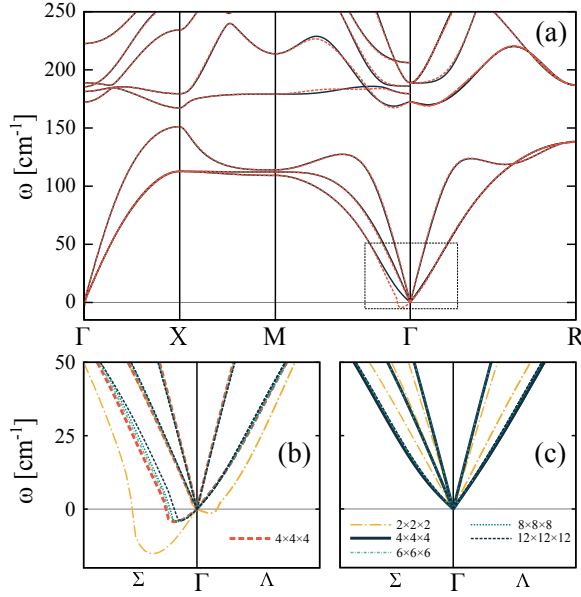


FIG. 1. (a) Phonon dispersion of BaTiO₃ calculated using the standard DD-based procedure (red dashed lines) and our higher-order interpolation scheme, based on Eq. (13) (black solid lines); a $4 \times 4 \times 4$ \mathbf{q} -points mesh was used in both cases. The bottom panels show a blow-up of the acoustic bands over the region marked by a dashed rectangle in (a). The additional (thinner) curves were obtained using different \mathbf{q} -points meshes [see the legend of (c)], either with the standard procedure (b) or Eq. (13) (c).

relaxed to its well-known low-temperature rhombohedral structure.

The black-solid lines of Fig 1(a) were calculated based on our higher-order multipolar interpolation scheme of Eq. (13). Remarkably, imaginary frequencies disappear even for the coarsest $2 \times 2 \times 2$ \mathbf{q} -grid (see Fig. 1(c)), and the dispersion of all acoustic branches shows optimal convergence already for a $4 \times 4 \times 4$ mesh. Our revised scheme seems to improve the description of some optical branches as well, most notably of the lowest-energy (ferroelectric) mode along the Γ -M and the Γ -R directions, although the corrections appear to be comparatively less important.

To make the above statements more quantitative, we extract the propagation velocities of the three acoustic waves from the dispersion curves of Fig. 1, and compare them with the macroscopic results, based on Eqs. (4), (7) and (8) (values are reported in Tab. S.V [25]). The velocities along the [110] direction are shown in Fig. 2 (data along [100] and [111] can be found in Fig. S.1 [25]) as a function of the \mathbf{q} -point mesh resolution. In order to illustrate the effect of each individual multipolar term, we have recalculated the sound velocity several times by progressively incorporating an increasing number of the terms at the rhs of Eq. (13). Incorporation of the DQ interactions drastically improves the accuracy of the es-

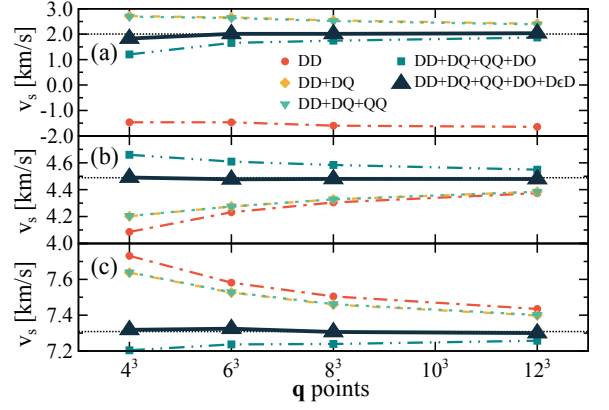


FIG. 2. Velocity of sound of the three acoustic branches along the [110] direction as a function of the \mathbf{q} -point mesh resolution. Dotted horizontal lines indicate the reference value of the sound velocity, obtained from macroscopic elasticity via Eqs. (4), (7) and (8). Different symbols (lines are a guide to the eye) show the velocities as obtained by considering an increasing number of multipolar interactions in Eq. (13).

timated velocity of sound, completely removing the spurious imaginary modes along all directions, as we said. However, only treating electrostatic terms up to $O(q^1)$ clearly does not guarantee accurate results in this case. Indeed, such an approximation leads to an error of the order of 10-20% in the velocities that decays only slowly as a function of the \mathbf{q} -grid resolution.

Including the $O(q^2)$ electrostatic interactions produces a further, remarkable improvement in the accuracy: the dispersion of the acoustic branches is essentially converged to the correct sound velocity already at a \mathbf{q} -mesh resolution of $4 \times 4 \times 4$. This result clearly supports our formal arguments of the previous paragraphs. Interestingly, among the three $O(q^2)$ interactions QQ have a negligible effect, which is a bit surprising considering that QQ terms should play an important role in piezoelectrics. This is likely due to the fact that the piezoelectric coefficients in ferroelectric materials such as BaTiO₃ are dominated by lattice-mediated contributions, while clamped-ion effects are comparatively negligible. [QQ interactions microscopically embody the contribution of $\bar{\mathbf{e}}$ to the dynamics of acoustic waves, see Eq.(S.22).] Indeed for BaTiO₃ we obtain a difference of one order of magnitude between both contributions (see Tab. S.VI [25]). To verify the validity of this hypothesis, we tested our method on a different material, GaP. In zincblende semiconductors the lattice-mediated and clamped-ion contributions to the piezoelectric tensor are generally similar in magnitude and opposite in sign (see, e.g., Tab. S.VI [25]), which makes GaP an excellent counterexample. And indeed, as we show in Fig. S.2 [25], DQ and QQ corrections are nearly equal and opposite, confirming our arguments above.

To assess the impact of our method on the calcula-

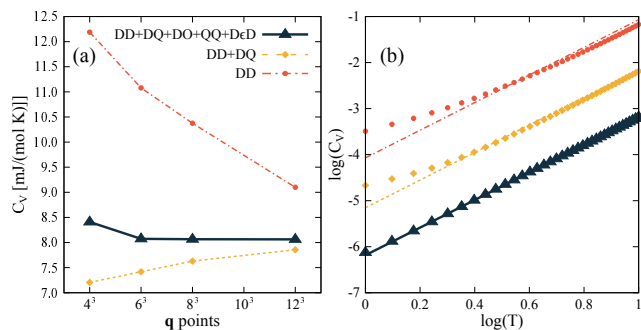


FIG. 3. (a) Specific heat (C_V) computed at $T = 5$ K from the phonon energy spectrum as a function of the coarse \mathbf{q} -point mesh by using three different interpolation methods (see text). (b) $\log(C_V)$ vs $\log(T)$ data obtained with a $12 \times 12 \times 12$ coarse mesh. Lines show a logarithmic fit to the Debye law, $C_V \propto T^3$. Vertical labels correspond to the DD data, the other two sets have been shifted by -1 and -2 for clarity. A fine \mathbf{q} -mesh of $40 \times 40 \times 40$ is used for the integration in all cases.

tion of thermal properties, we have computed the low-temperature specific heat [7] of rhombohedral BaTiO_3 . In Fig. 3(a) we show the calculated values of C_V ($T = 5$ K) as a function of the \mathbf{q} -mesh resolution. Our method, as expected, yields a dramatically improved convergence rate compared to the standard DD-based treatment. Note that inclusion of the DQ interactions already reduces the error by approximately one order of magnitude. In Fig. 3(b) we show a log-log plot of $C_V(T)$, ($T = 0.25 - 10$ K) calculated at fixed mesh resolution of $12 \times 12 \times 12$. By using our higher-order method, the results accurately reproduce the low-temperature limit ($\sim T^3$) of Debye's law; [34] the fitted Debye temperature, $T_D = 530$ K, is in good agreement with existing experimental and theoretical values. [35] Conversely, the standard DD-based approach shows important deviations, pointing to a *qualitative*, rather than quantitative, misrepresentation of the low-energy part of the phonon spectrum. Interestingly, DQ terms alone are clearly unable to correct this flaw, indicating that the absence of spurious imaginary branches is not *per se* sufficient to guarantee that the relevant physical properties are well represented.

To summarize, by including higher-order multipolar interactions in the determination of interatomic force constants we were able to eliminate spurious artifacts in the phonon dispersion spectrum of BaTiO_3 , and obtain a remarkably accurate description of the acoustic branches even at small \mathbf{q} -mesh resolutions. Unphysical acoustic imaginary modes are not exclusive of the BaTiO_3 system studied here. Indeed, materials databases, such as Refs. 21 or 36, are riddled with piezoelectrics developing this kind of artifacts. The implementation shown here can be readily applied for improving the high-throughput generation of phonon band structures to be included in

these and other databases.

We acknowledge the support of Ministerio de Economía, Industria y Competitividad (MINECO-Spain) through Grants No. MAT2016-77100-C2-2-P and No. SEV-2015-0496, and of Generalitat de Catalunya (Grant No. 2017 SGR1506). This project has received funding from the European Research Council (ERC) under the European Union's Horizon 2020 research and innovation program (Grant Agreement No. 724529). Part of the calculations were performed at the Supercomputing Center of Galicia (CESGA).

* mroyo@icmab.es

† mstengel@icmab.es

- [1] A. Fleszar and Xavier Gonze, "First-principles thermodynamical properties of semiconductors," *Physical Review Letters* **64**, 2961 (1990).
- [2] D. A. Broido, M. Malorny, G. Birner, Natalio Mingo, and D. A. Stewart, "Intrinsic lattice thermal conductivity of semiconductors from first principles," *Applied Physics Letters* **91**, 231922 (2007).
- [3] A. Ward, D. A. Broido, Derek A. Stewart, and G. Deinzer, "Ab initio theory of the lattice thermal conductivity in diamond," *Phys. Rev. B* **80**, 125203 (2009).
- [4] A. Ward and D. A. Broido, "Intrinsic phonon relaxation times from first-principles studies of the thermal conductivities of Si and Ge," *Phys. Rev. B* **81**, 085205 (2010).
- [5] Giorgia Fugallo, Michele Lazzeri, Lorenzo Paulatto, and Francesco Mauri, "Ab initio variational approach for evaluating lattice thermal conductivity," *Phys. Rev. B* **88**, 045430 (2013).
- [6] Wu Li, Jesús Carrete, Nebil A. Katcho, and Natalio Mingo, "ShengBTE: A solver of the Boltzmann transport equation for phonons," *Computer Physics Communications* **185**, 1747–1758 (2014).
- [7] Changyol Lee and Xavier Gonze, "Ab initio calculation of the thermodynamic properties and atomic temperature factors of SiO_2 α -quartz and stishovite," *Phys. Rev. B* **51**, 8610–8613 (1995).
- [8] M. Sanati and S. K. Estreicher, "Specific heat and entropy of GaN," *Journal of Physics: Condensed Matter* **16**, L327–L331 (2004).
- [9] Feliciano Giustino, "Electron-phonon interactions from first principles," *Rev. Mod. Phys.* **89**, 015003 (2017).
- [10] Stefano Baroni, Paolo Giannozzi, and Andrea Testa, "Green's-function approach to linear response in solids," *Physical Review Letters* **58**, 1861–1864 (1987).
- [11] Xavier Gonze, "Adiabatic density-functional perturbation theory," *Physical Review A* **52**, 1096–1114 (1995).
- [12] Xavier Gonze, "Erratum: Adiabatic density-functional perturbation theory," *Physical Review A* **54**, 4591–4591 (1996).
- [13] Stefano Baroni, Stefano De Gironcoli, Andrea Dal Corso, and Paolo Giannozzi, "Phonons and related crystal properties from density-functional perturbation theory," *Reviews of Modern Physics* **73**, 515–562 (2001).
- [14] Paolo Giannozzi, Stefano De Gironcoli, Pasquale Pavone, and Stefano Baroni, "Ab initio calculation of phonon dispersions in semiconductors,"

- Physical Review B **43**, 7231–7242 (1991).
- [15] Xavier Gonze, “First-principles responses of solids to atomic displacements and homogeneous electric fields: Implementation of a conjugate-gradient algorithm,” *Physical Review B* **55**, 10337–10354 (1997).
 - [16] Xavier Gonze and Changyol Lee, “Dynamical matrices, Born effective charges, dielectric permittivity tensors, and interatomic force constants from density-functional perturbation theory,” *Physical Review B* **55**, 10355–10368 (1997).
 - [17] William Cochran, “Lattice dynamics of sodium,” *Proceedings of the Royal Society of London. Series A. Mathematical and Physical Sciences* **276**, 308–323 (1963).
 - [18] Atsushi Togo, Fumiyasu Oba, and Isao Tanaka, “First-principles calculations of the ferroelastic transition between rutile-type and CaCl_2 -type SiO_2 at high pressures,” *Phys. Rev. B* **78**, 134106 (2008).
 - [19] Hugo Aramberri, Riccardo Rurali, and Jorge Íñiguez, “Thermal conductivity changes across a structural phase transition: The case of high-pressure silica,” *Phys. Rev. B* **96**, 195201 (2017).
 - [20] P. Hermet, A. Lignie, G. Frayssé, P. Armand, and Ph. Papet, “Thermodynamic properties of the α -quartz-type and rutile-type GeO_2 from first-principles calculations,” *Phys. Chem. Chem. Phys.* **15**, 15943–15948 (2013).
 - [21] Atsushi Togo, *phonondb@kyoto-u* (2015 (accessed April 14, 2020)), <http://phonondb.mtl.kyoto-u.ac.jp>.
 - [22] Max Born and Kun Huang, *Dynamical theory of crystal lattices* (Oxford University Press, Oxford, 1954) p. 420.
 - [23] Massimiliano Stengel, “Flexoelectricity from density-functional perturbation theory,” *Physical Review B* **88**, 174106 (2013).
 - [24] Massimiliano Stengel, “Unified *ab initio* formulation of flexoelectricity and strain-gradient elasticity,” *Physical Review B* **93**, 245107 (2016).
 - [25] See Supplemental Material at <http://link> for more information about computational details and results.
 - [26] Xifan Wu, David Vanderbilt, and D. R. Hamann, “Systematic treatment of displacements, strains, and electric fields in density-functional perturbation theory,” *Phys. Rev. B* **72**, 035105 (2005).
 - [27] Jiawang Hong and David Vanderbilt, “First-principles theory and calculation of flexoelectricity,” *Phys. Rev. B* **88**, 174107 (2013).
 - [28] Z. Li, M. Grimsditch, C.M. Foster, and S.-K. Chan, “Dielectric and elastic properties of ferroelectric materials at elevated temperature,” *Journal of Physics and Chemistry of Solids* **57**, 1433–1438 (1996).
 - [29] Abo-el-nour N. Abd-Alla and Nadia A. Askar, “Calculation of Bulk Acoustic Wave Propagation Velocities in Trigonal Piezoelectric Smart Materials,” *Applied Mathematics and Information Sciences* **8**, 1625–1632 (2014).
 - [30] Richard M. Martin, “Piezoelectricity,” *Physical Review B* **5**, 1607–1613 (1972).
 - [31] Miquel Royo and Massimiliano Stengel, “First-Principles Theory of Spontaneous Displacements, Quadrupoles and Flexoelectricity,” *Phys. Rev. X* **9**, 021050 (2019).
 - [32] Aldo H. Romero, Douglas C. Allan, Bernard Amadon, Gabriel Antonius, Thomas Applencourt, Lucas Baguet, Jordan Bieder, François Bottin, Johann Bouchet, Eric Bousquet, Fabien Bruneval, Guillaume Brunin, Damien Caliste, Michel Côté, Jules Denier, Cyrus Dreyer, Philippe Ghosez, Matteo Giantomassi, Yannick Gillet, Olivier Gingras, Donald R. Hamann, Geoffrey Hautier, François Jollet, Gérald Jomard, Alexandre Martin, Henrique P. C. Miranda, Francesco Naccarato, Guido Petretto, Nicholas A. Pike, Valentin Planes, Sergei Prokhorenko, Tonatiuh Rangel, Fabio Ricci, Gian-Marco Rignanese, Miquel Royo, Massimiliano Stengel, Marc Torrent, Michiel J. van Setten, Benoit Van Troeye, Matthieu J. Verstraete, Julia Wiktor, Josef W. Zwanziger, and Xavier Gonze, “ABINIT: Overview and focus on selected capabilities,” *The Journal of Chemical Physics* **152**, 124102 (2020).
 - [33] Xavier Gonze, J.-C. Charlier, D.C. Allan, and M.P. Teter, “Interatomic force constants from first principles: The case of α -quartz,” *Physical Review B* **50**, 13035–13038 (1994).
 - [34] Charles Kittel, *Introduction to Solid State Physics*, 6th ed. (John Wiley & Sons, Inc., New York, 1986).
 - [35] S. Sanna, C. Thierfelder, S. Wippermann, T. P. Sinha, and W. G. Schmidt, “Barium titanate ground- and excited-state properties from first-principles calculations,” *Phys. Rev. B* **83**, 054112 (2011).
 - [36] Henrique P. C. Miranda, “Phonon Website,” (2015 (accessed April 14, 2020)), <http://henriquemiranda.github.io/phononwebsite>.